



HAL
open science

First results of the PML monitor of atmospheric turbulence profile with high vertical resolution

A. Ziad, F. Blary, J. Borgnino, Y. Fanteï-Caujolle, E. Aristidi, F. Martin, H. Lantéri, R. Douet, E. Bondoux, D. Mekarnia

► **To cite this version:**

A. Ziad, F. Blary, J. Borgnino, Y. Fanteï-Caujolle, E. Aristidi, et al.. First results of the PML monitor of atmospheric turbulence profile with high vertical resolution. *Astronomy and Astrophysics - A&A*, 2013, 559, pp.L6. 10.1051/0004-6361/201322468 . hal-02453255

HAL Id: hal-02453255

<https://hal.science/hal-02453255>

Submitted on 17 Nov 2022

HAL is a multi-disciplinary open access archive for the deposit and dissemination of scientific research documents, whether they are published or not. The documents may come from teaching and research institutions in France or abroad, or from public or private research centers.

L'archive ouverte pluridisciplinaire **HAL**, est destinée au dépôt et à la diffusion de documents scientifiques de niveau recherche, publiés ou non, émanant des établissements d'enseignement et de recherche français ou étrangers, des laboratoires publics ou privés.

LETTER TO THE EDITOR

First results of the PML monitor of atmospheric turbulence profile with high vertical resolution

A. Ziad, F. Blary, J. Borgnino, Y. Fanteï-Caujolle, E. Aristidi, F. Martin, H. Lantéri, R. Douet, E. Bondoux, and D. Mékarnia

Laboratoire J.L. Lagrange UMR 7293, Université de Nice Sophia-Antipolis/CNRS/OCA, 06108 Parc Valrose, Nice, France
e-mail: ziad@unice.fr

Received 9 August 2013 / Accepted 23 September 2013

ABSTRACT

Aims. Future extremely large telescopes will certainly be equipped with wide-field adaptive optics systems. The optimization of the performances of these techniques requires a precise specification of the different components of these AO systems. Most of these technical specifications are related to the atmospheric turbulence parameters, particularly the profile of the refractive index structure constant $C_N^2(h)$. A new monitor called Profiler of Moon Limb (PML) for the extraction of the $C_N^2(h)$ profile with high vertical resolution and its first results are presented.

Methods. The PML instrument uses an optical method based on the observation of the Moon limb through two subapertures. The use of the lunar limb leads to a continuum of double stars allowing a scan of the whole atmosphere with high resolution in altitude.

Results. The first prototype of the PML has been installed at Dome C in Antarctica and the first results of the PML are presented and compared to radio-sounding balloon profiles. In addition to the $C_N^2(h)$ profile obtained with high vertical resolution, PML is also able to provide other atmospheric turbulence parameters such as the outer scale profile, the total seeing, and the isoplanatic and isoplanetic angles.

Key words. atmospheric effects – turbulence – site testing – instrumentation: adaptive optics

1. Introduction

For the next generation of ground-based telescopes, the classical adaptive optics (AO) reaches its limitations mainly when correction is needed over a large field of view. Other AO concepts called wide-field adaptive optics (WFAO) have been proposed for this large field compensation in the perspective of future ELTs (Ellerbroek 2011; Hubin 2011). The optimization of the performances of the WFAO techniques requires a precise specification of the different components of these systems. Some of these technical specifications are related to the optical parameters of the atmospheric turbulence, particularly the $C_N^2(h)$ profile. Moreover, recent studies (Costille & Fusco 2011) show that it is necessary to have access to $C_N^2(h)$ profiles with high vertical resolution for a better evaluation of the performance of a WFAO system.

Different instruments such as radio-sounding balloons, SCIDAR, MASS, SLODAR, and MOSP have been developed for $C_N^2(h)$ profile estimation. The balloons (Azouit et al. 2005) lead to estimated profiles with high vertical resolution, but the measurements are sequential over the ascent time ~ 2 h and they are expensive because they are lost after the flight. The SCIDAR (Fuchs et al. 1998) requires a large telescope (~ 2 m) and the resolution is low in the ground layer (GL). The other instruments lead to a low altitude resolution and/or are restricted to a part of the atmosphere, either GL or free atmosphere (FA).

A new instrument called Profiler of Moon Limb (PML) initially known as Profiler Bord Lunaire (PBL) has been developed for the extraction of the $C_N^2(h)$ profile with high vertical resolution from lunar limb fluctuations. The PML instrument is based on a differential method by observation of the lunar limb through two sub-apertures. The advantage of using the lunar

limb is the presence of a continuum of double stars allowing the scan of the whole atmosphere with high resolution.

In this paper, the PML instrument is presented and its components are described. The theoretical background of the extraction of $C_N^2(h)$ profile from PML measurements is presented. The PML instrument was installed at Dome C in Antarctica in January 2011. The first results of PML obtained during this campaign are presented and compared to radio-sounding balloon profiles.

2. PML instrument

The PML is a new instrument for the extraction of the C_N^2 profile with high vertical resolution that uses an optical method based on the observation of the Moon limb. This has the advantage of offering a large number of angular separations required between two points of the edge allowing the scan of the atmosphere with a very fine resolution. The PML instrument uses the differential method of a differential image motion monitor (DIMM; Sarazin & Roddier 1990) based this time on the observation of the lunar limb instead of a bright single star, through two sub-apertures (Fig. 1). The angular correlation along the lunar limb of the differential distance between the two lunar edges leads to the $C_N^2(h)$ profile. Other parameters of turbulence are also accessible from this instrument such as the profile of outer scale (Maire et al. 2007), the seeing, and the isoplanatic and isoplanetic angles (Elhalkouj et al. 2008).

The principle of the PML instrument is based on the measurement of the angular correlation of the fluctuation differences in the wavefront angle-of-arrival (AA) deduced from the motion of the Moon's limb image. The AA fluctuations are measured



Fig. 1. The PML instrument at Dome C, Antarctica in January 2011. The top-left insert shows the subapertures mask of PML.

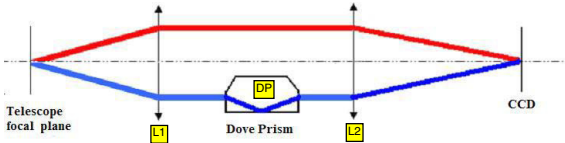


Fig. 2. The optical device of the PML instrument.

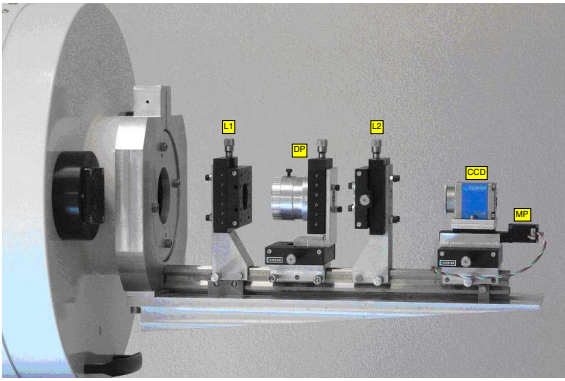


Fig. 3. Focal plane instrument of PML.

perpendicularly to the lunar limb leading to transverse correlations for different angular separations along the Moon.

The PML instrument consists of a 16-inch telescope (Meade M16) which is installed on an Astrophysics AP3600 mount (Fig. 1). This mount was chosen to avoid overload especially in Dome C conditions. For temperate sites we use an AP1200 mount which is lighter and cheaper. The pupil mask composed of two sub-apertures of diameter $D = 6$ cm separated by a baseline $B = 26.7$ cm, is placed at the entrance pupil of the telescope. The optical device of the PML consists of a collimated beam by using a first lens L1 placed at its focal length from the telescope focus (Figs. 2 and 3). Two parallel beams are formed at the output of L1 corresponding to each sub-aperture. A Dove prism (DP) is placed on one of the two beams to reverse one of two images of the lunar edge in order to avoid overlapping bright parts of the Moon (Fig. 4). A second lens L2 is used to form the two images of the Moon limb on a PCO PixelFly CCD camera. Each optical element is placed on a Micro-control plate allowing fine adjustments. To compensate for variations in the telescope's focus because of the temperature variations, we installed the CCD camera on an automatic micro-control plate (MP; Fig. 3) controlled by software.

Images at the focal plane (Fig. 4) are recorded using a PixelFly CCD camera with 640×480 pixel matrix and

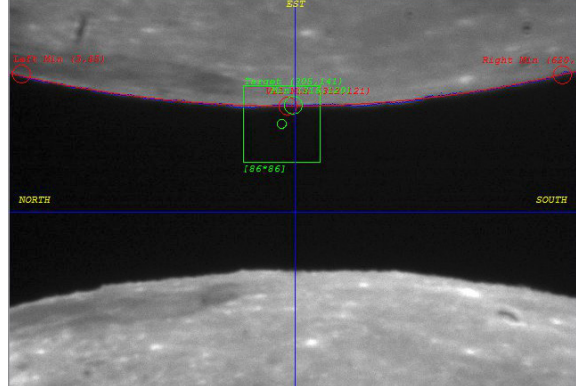


Fig. 4. Example of PML data acquisition.

(9.9×9.9) μm^2 pixel size. The dynamic range of the analog/digital conversion is 12 bits. The readout noise is $12 e^-$ rms and the imaging frequency is 33 Hz. In order to freeze atmospheric effects on the motion of the Moon's limb image and to have enough flux, the exposure time was set to 5 ms. The spectral response of the camera is maximum for $\lambda = 0.5 \mu\text{m}$ in a 375–550 μm range.

3. Theoretical background

The observation of the lunar limb through two sub-apertures presents two configurations when looking at the edge in a direction parallel or perpendicular to the baseline. We use the first configuration to extract the C_N^2 vertical distribution (top-left insert of Fig. 1).

The transverse covariance of the difference of AA fluctuations α between the two images of the Moon limb (Fig. 4) corresponds to

$$C_{\Delta\alpha}(\theta) = \langle [\alpha(r, \theta_0) - \alpha(r+B, \theta_0)] [\alpha(r, \theta_0 + \theta) - \alpha(r+B, \theta_0 + \theta)] \rangle, \quad (1)$$

where $B = 26.7$ cm is the baseline between the subapertures, θ is the angular separation along the Moon limb, and θ_0 is assumed equal to zero. After development, this expression is a function of spatial covariances integrated over the altitude h of the turbulent layers of the whole atmosphere

$$C_{\Delta\alpha}(\theta) = \int dh C_N^2(h) K_\alpha(B, h, \theta), \quad (2)$$

where

$$K_\alpha(B, h, \theta) = 2 C_\alpha(\theta h) - C_\alpha(B - \theta h) - C_\alpha(B + \theta h). \quad (3)$$

In this equation C_α is the normalized spatial covariance which in the case of the von Kàrmàn model for a baseline ϱ , a sub-aperture diameter D (here 6 cm), and a single layer at altitude h is given by Avila et al. (1997) as

$$C_\alpha(\varrho) = 1.19 \sec(z) \int df f^3 \left(f^2 + \frac{1}{\mathcal{L}_0(h)^2} \right)^{-11/6} \times [J_0(2\pi f \varrho) + J_2(2\pi f \varrho)] \left[2 \frac{J_1(\pi D f)}{\pi D f} \right]^2, \quad (4)$$

where f is the modulus of the spatial frequency, z is the zenithal distance and \mathcal{L}_0 is the outer scale.

Equation (3) represents for a single layer a spatial covariance triplet similar to the SCIDAR one (Fuchs et al. 1998) which is

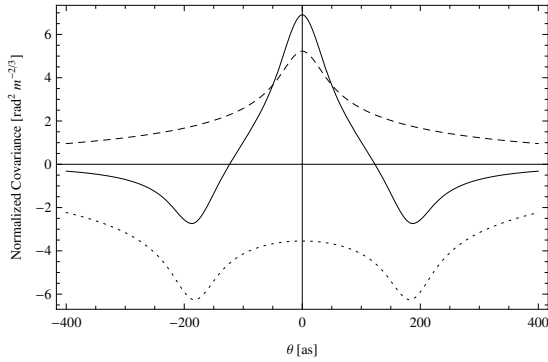


Fig. 5. Triplet of spatial covariances for a single turbulent layer localized at an altitude $h = 300$ m (solid line). The dashed line indicates the central spatial covariance $C_\alpha(\theta h)$ in Eq. (3). The dotted line indicates the difference $[K_\alpha(B, h, \theta) - 2 C_\alpha(\theta h)]$ leading to lateral peaks $[-C_\alpha(B - \theta h) - C_\alpha(B + \theta h)]$.

shown in Fig. 5 for a turbulent layer localized at $h = 300$ m. The position of the lateral peak ($B = \theta h$) defines the altitude of the layer so that its height leads to the contribution of this layer to the $C_N^2(h)$ profile. For the whole atmosphere we have the superposition of triplets corresponding to the different turbulent layers. The central covariance $C_\alpha(\theta h)$ in Eq. (3) could hide the lateral peaks (dotted curve in Fig. 5) particularly for high layers (small θ) and could be estimated separately from one Moon limb. One can have two estimates of this central covariance from each Moon limb and use the mean one. The subtraction of $2 \times C_\alpha(\theta h)$ from the triplet in Eq. (3) leads directly to lateral peaks $[-C_\alpha(B - \theta h) - C_\alpha(B + \theta h)]$. For the whole atmosphere we have the superposition of these lateral peaks with different positions and weightings corresponding to the different turbulent layers in the atmosphere.

Thus, the extraction of the $C_N^2(h)$ profile from the PML is obtained from the estimation of the lateral peaks of the whole atmosphere obtained by this difference:

$$Y(\theta) = C_{\Delta\alpha}(\theta) - 2 \times \int dh C_N^2(h) C_\alpha(\theta h). \quad (5)$$

In a matrix form, one can write

$$Y = M \times c, \quad (6)$$

where c is a vector of the sampled $C_N^2(h_i)$ profile and M is a matrix obtained from the difference $[K_\alpha(B, h_i, \theta_j) - 2 C_\alpha(\theta_j h_i)]$ for different altitudes h_i and angular separations θ_j .

4. Data processing and results

The first step of PML data processing is to accurately retrieve the AA fluctuations from the Moon's limb motion (transverse AA fluctuations). After processing a flat and dark field correction, each image $I(x, y)$ is slightly blurred with a median filter on 3×3 pixel blocks. This removes the possibility that outliers due to Poisson noise or to small features of the Moon with relative high intensity differences can affect the detection of the limb. This type of filtering is more effective than convolution when the goal is to simultaneously reduce noise and preserve edges (Pratt 1978).

Then, the image with the two lunar limbs is separated on two images with top and bottom edges (Fig. 4). On each half-image, a spatial gradient $G(x, y)$ is processed by convolution with a 3×3

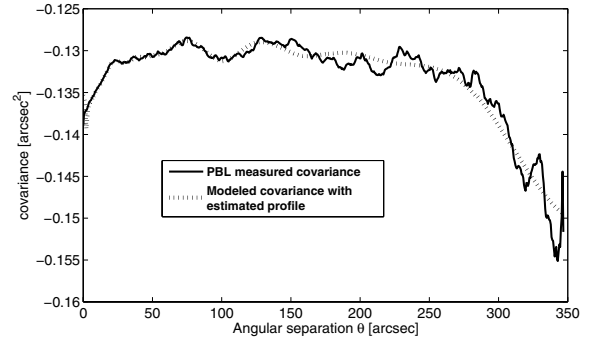


Fig. 6. Example of lateral covariance $Y(\theta)$ obtained with PML at Dome C in Antarctica on January 25, 2011 at 16h45 UT (solid line). The PML extracted $C_N^2(h)$ profile is obtained by modeling angular covariance (dotted line) leading to the best fit of the measured covariance (solid line).

Prewitt edge detector (Pratt 1978) defined as $P = \begin{pmatrix} -1 & -1 & -1 \\ 0 & 0 & 0 \\ 1 & 1 & 1 \end{pmatrix}$,

or $-P$ if the y -axis points to the Moon center. Detection of the limb position in absolute value of the image gradient is determined by a centroid calculation over each column.

We process $N = 1000$ images (acquisition of 1 min) that give two sets of Moon limb angular positions corresponding to the top and bottom of the lunar edge in Fig. 4. Then, a transverse covariance of the difference of the AA fluctuations $C_{\Delta\alpha}(\theta)$ between these two Moon limbs as given in Eq. (1) is deduced. This differential covariance calculated for each image has the practical advantage of being insensitive to vibration effects of the telescope, wind shaking, and tracking errors. On the other hand, from top and bottom limbs, we deduce separately two estimations of the central covariance $C_\alpha(\theta h)$ integrated over the whole atmosphere. Twice of the mean of these central covariances is then subtracted from $C_{\Delta\alpha}(\theta)$ as indicated in Eq. (5) leading to the lateral covariance estimator Y (Fig. 6). This estimator and all the covariances are obtained for each pixel along ~ 620 pixels of the CCD camera (~ 20 pixels are lost when recentering Moon limbs on the CCD owing to the mount drift). Each pixel corresponds to $\approx 0.57''$ leading to a total field of more than $350''$.

Retrieving the $C_N^2(h)$ profile from the transverse covariance estimator Y is an inverse problem as indicated in Eq. (6). The estimated $C_N^2(h)$ is obtained by minimization of the least squares criterion $J = \|Y - Mc\|^2$ under positivity constraint using an iterative gradient method (Bertero & Boccacci 1998). A diagonal weighting matrix with Y variances is used to favor the steadier measurement.

The PML instrument was first installed at the Dome C site in Antarctica for a long campaign measurement for the whole year 2011. But owing to a very limited Internet connection at the Concordia station, we did not have access to the PML database. We had to wait for the summer campaign to recover it (May 2012). Since this time, the data processing of this campaign has been continuously in progress and an example of the first profiles obtained on two data sets are shown in Fig. 7 compared to median profile of radio-sounding balloons obtained during the 2005 winter campaign (Trinquet et al. 2008). The variations of the balloon data are represented by the 10% and 90% percentiles of the measured profiles during this 2005 campaign (dotted lines in Fig. 7). A direct comparison of these results is meaningless, but these first results show that the instantaneous measurements of PML are consistent with the general behavior of the Dome C atmosphere as indicated by radio-sounding

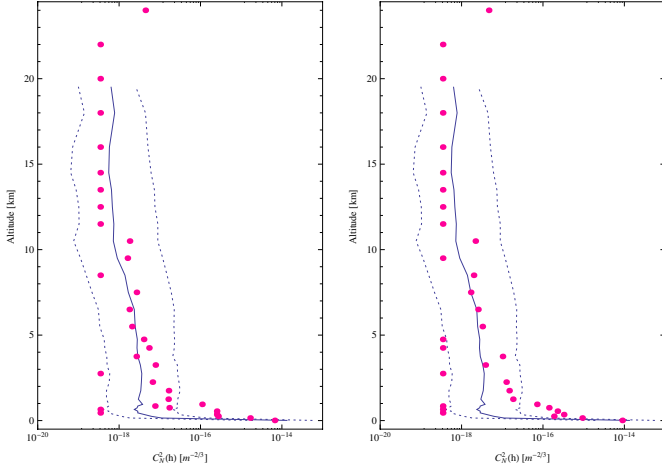


Fig. 7. Example of C_N^2 profile (dots) from PML at Dome C in Antarctica on January 25, 2011 at 16h45UT (left panel) and 17h17 (right panel). For comparison, the median profile (solid line) of radio-sounding balloons obtained during the 2005 winter campaign is plotted in solid line. Dotted lines indicate the 10% and 90% percentiles of the balloon data.

balloon profiles. Indeed, the Fried parameter deduced from the PML profile in Fig. 7 is $r_0 = 8.2$ cm for the 16h45UT profile and $r_0 = 7.5$ cm for 17h17UT, while the median balloon profile from the 2005 campaign leads to $r_0 = 6.7$ cm. Figure 6 shows the measured lateral covariance $Y(\theta)$ (solid line) as indicated in Eq. (5). We note that for large θ , the measured covariance $Y(\theta)$ shows greater fluctuation because of the smaller sample size.

The $C_N^2(h)$ profiles in Fig. 7 were deduced by comparing the measured lateral covariance $Y(\theta)$ and the modeled one (Fig. 6). These profiles (Fig. 7) were obtained with a variable vertical resolution. Indeed, the altitude is inversely proportional to the angular separation θ with a maximum of more than $350''$. Then, the resolution is higher in the ground layer than in the free atmosphere. The resolution used for the first Dome C results (Fig. 7) is $\Delta h = 100$ m for the ground layer ($h \leq 1$ km), $\Delta h = 500$ m for the low free atmosphere ($1 \text{ km} < h < 5$ km), $\Delta h = 1000$ m for the mid-free atmosphere ($5 \text{ km} < h < 15$ km), and $\Delta h = 2000$ m for the high free atmosphere ($h > 15$ km). The highest altitude h_{\max} measured with the PML is more than 50 km. However, we limited h_{\max} to 25 km for comparison with balloon profiles reaching only 20 km (Fig. 7). On the other hand, because of a limited field of view the PML instrument has a minimum altitude detectable. Indeed, the maximum of the lateral peak (Fig. 5) detectable is around 150 m for the field of view of PML which is more than $350''$ ($B = \theta h$). As shown in Fig. 5, even if the maximum of lateral peak is not in the field of view, the corresponding layer is detectable if we take into account the expansion of the covariance curves. Then, if we consider an outer scale of 10–100 m (baseline at which the spatial covariance in Eq. (4) tends to zero), the minimum altitude is fixed to 100 m. The contribution of the lowest layer 0–100 m is obtained by the difference between the profile deduced from the inversion of the PML covariances (Fig. 6) and the total seeing from DIMM method (Sarazin & Roddier 1990) using PML data. For the total seeing obtained from PML, we have about 620 estimations (each point of the Moon limb leads to a DIMM measurement) and we keep only the median one.

The error sources of PML monitor are similar to those affecting the MOSP instrument which are described in detail in Sect. 3.3 of Maire et al. 2007. These errors are mainly related to the detection of the Moon limb position and are due to photon

noise. For the evaluation of the error of this photon noise we used the same simulation described in Maire et al. 2007. The Moon limb images are simulated by a 2D Heaviside function. The Fourier Transform (FT) of this function is multiplied by the atmospheric short-exposure transfer function to introduce the seeing conditions and by the aperture transfer function. The 2D inverse FT of this product leads to simulated images of the Moon's limb for given seeing conditions and PML aperture filtering. Then, the photon noise is added as Poisson distribution using the mean value of intensity of each pixel as obtained with the PML observations. These Moon limb images pass through the PML data processing described in Sect. 4. The lateral covariance in Eq. (5) of the Moon limb fluctuations due to photon noise is calculated for each realization and the mean covariance is deduced from $N = 1000$ samples. As Moon limb fluctuations due to photon error and atmospheric turbulence are considered uncorrelated, this lateral covariance is added to the theoretical covariance using Eqs. (2), (4), and (5), and the median radio-sounding balloon profile (Fig. 7). The error on the lateral covariance due to the photon noise is at maximum 0.5% in the seeing conditions of the results presented in Fig. 7. The noisy lateral covariance is then inverted to retrieve the $C_N^2(h)$ profile as in the PML instrument. Comparisons with the injected profile which is no more than the median profile $C_{N,\text{Bal}}^2(h)$ of radio-sounding balloons is evaluated using a relative error defined as $E_{\text{ph}} = \sum_{i=1}^n |C_{N,\text{Bal}}^2(h_i) - C_N^2(h_i)| / \sum_{i=1}^n C_N^2(h_i)$ over n retrieved layers. Here, E_{ph} is about 4% representing a typical low error for this kind of instrument.

5. Conclusions

The advantage of the PML instrument is that in addition to the $C_N^2(h)$ profile extracted with high vertical resolution using an easy and undemanding technique, it is able to provide other parameters of turbulence, particularly the profile of the outer scale using the same technique described in Maire et al. 2007. Estimations of the isoplanatic and isopistonc domains (Elhalkouj et al. 2008) from the PML instrument are also possible. Furthermore, the PML is also applicable to solar limb by use of a density filter. The first PML results obtained with solar limb at Dome C are also available. These results and those of other turbulence parameters will be submitted for future publication in separate papers.

Acknowledgements. We would like to thank the Polar Institutes IPEV and PNRA, the National Institute for Earth Sciences and Astronomy INSU, and the French Programme of High Angular Resolution ASHRA for logistical and financial support for the development and the installation of the PML instrument at the site of Dome C in Antarctica. We also wish to thank warmly Alex Robini for his precious help and we are very grateful for his dedication to the success of the PML. We thank the technical team of the Winterover 2011 for their help.

References

- Avila, R., Ziad, A., Borgnino, J., et al. 1997, *J. Opt. Soc. Am. A*, 14, 3070
- Azouit, M., & Vernin, J. 2005, *PASP*, 117, 536
- Bertero, M. & Boccacci, P. 1998, *Introduction to inverse Problems in imaging* (Bristol: IOP Publishing)
- Costille, A., & Fusco, T. 2011, in 2nd Int. Conf. AO4ELT, Victoria
- Elhalkouj, T., Ziad, A., Petrov, R. G., et al. 2008, *A&A*, 477, 337
- Ellerbroek, B. 2011, in 2nd Int. Conf. AO4ELT, Victoria
- Fuchs, A., Tallon, M., & Vernin, J. 1998, *PASP*, 110, 86
- Hubin, N. 2011, in 2nd Int. Conf. AO4ELT, Victoria
- Maire, J., Ziad, A., Borgnino, J., et al. 2007, *MNRAS*, 377, 236
- Pratt, W. K. 1978, *Digital Image Processing* (New York: Wiley-Interscience)
- Sarazin, M., & Roddier, F. 1990, *A&A*, 227, 294
- Trinquet, H., Agabi, A., Vernin, J., et al. 2008, *PASP*, 120, 203